Discovery of Radio Afterglow from the Most Distant Cosmic Explosion

Submitted to ApJ Letters

Discovery of Radio Afterglow from the Most Distant Cosmic Explosion

Poonam Chandra[1], Dale A. Frail[2], Derek Fox[3], Shrinivas Kulkarni[4], Edo Berger[5], S. Bradley Cenko[6], Douglas C.-J. Bock[7], Fiona Harrsion[4], Mansi Kasliwal[4]

ABSTRACT

We report the discovery of radio afterglow emission from the gamma-ray burst GRB 090423, which exploded at a redshift of 8.3, making it the object with the highest known redshift in the Universe. By combining our radio measurements with existing X-ray and infrared observations, we estimate the kinetic energy of the afterglow, the geometry of the outflow and the density of the circumburst medium. Our best fit model is a quasi-spherical, high-energy explosion in a low, constant-density medium. GRB 090423 had a similar energy release to the other well-studied high redshift GRB 050904 ($z = 6.26$), but their circumburst densities differ by two orders of magnitude. We compare the properties of GRB 090423 with a sample of GRBs at moderate redshifts. We find that the high energy and afterglow properties of GRB 090423 are not sufficiently different from other GRBs to suggest a different kind of progenitor, such as a Population III star. However, we argue that it is not clear that the afterglow properties alone can provide convincing identification of Population III progenitors. We suggest that the millimeter and centimeter radio detections of GRB 090423 at early

[1]Department of Physics, Royal Military College of Canada, Kingston, ON, Canada; Poonam.Chandra@rmc.ca

[2]National Radio Astronomy Observatory, 1003 Lopezville Road, Socorro, NM 87801.

[3]Department of Astronomy & Astrophysics, 525 Davey Laboratory, Pennsylvania State University, University Park, PA 16802.

[4]Department of Astronomy, California Institute of Technology, Pasadena, CA 91125.

[5]Harvard University, 60 Garden Street, Cambridge, MA 02138.

[6]Department of Astronomy, 601 Campbell Hall, University of California, Berkeley, CA 94720-3411.

[7]Combined Array for Research in Millimeter-wave Astronomy, P.O. Box 968, Big Pine, CA 93513.

times contained emission from a reverse shock component. This has important implications for the detection of high redshift GRBs by the next generation of radio facilities.

Subject headings: cosmology: observations—gamma rays: bursts—hydrodynamics—radio continuum: general—stars: early-type

1. Introduction

Because of their extreme luminosities GRBs are detectable out to large distances by current missions, and due to their connection to core collapse SNe (Woosley & Bloom 2006), they could in principal reveal the stars that form from the first dark matter halos ($z \sim$ 20–30) through to the epoch of reionization at $z = 11 \pm 3$ and closer (Lamb & Reichart 2000; Ciardi & Loeb 2000; Gou et al. 2004; Inoue et al. 2007). As bright continuum sources, GRB afterglows also make ideal backlights to probe the intergalactic medium as well as the interstellar medium in their host galaxies. Predicted to occur at redshifts beyond those where quasars are expected, they could be used to study both the reionization history and metal enrichment of the early universe (Totani et al. 2006).

The fraction of detectable GRBs that lie at high redshift ($z > 6$) is, however, expected to be small (<10%; Perley et al. 2009; Bromm & Loeb 2006). Until recently there were only two GRBs with measured redshifts $z > 6$; GRB 050904 (Kawai et al. 2006) and GRB 080913 (Greiner et al. 2009) with $z = 6.3$ and $z = 6.7$, respectively. However, on April 23, 2009 the *Swift* Burst Alert Telescope (BAT) discovered GRB 090423 and the on-board X-ray Telescope (XRT) detected and localized a variable X-ray afterglow (Tanvir et al. 2009a; Salvaterra et al. 2009). In ground-based follow-up observations no optical counterpart was found but a fading afterglow was detected by several groups at wavelengths longward of J band (1.2 μm). Based on both broadband photometry and near infrared (NIR) spectroscopy, the sharp optical/NIR drop off was argued to be due to the Lyman-α absorption in the intergalactic medium, consistent with a redshift with a best-fit value of $z = 8.26^{+0.07}_{-0.08}$ (Tanvir et al. 2009a). The high redshift of GRB 090423 makes it the most distant observed GRB, as well as the most distant object of any kind other than the Cosmic Microwave Background. This event occurred approximately 630 million years after the Big Bang, confirming that massive stellar formation occurred in the very early universe.

In this paper we report the discovery of the radio afterglow from GRB 090423 with

the Very Large Array[1] (VLA). Broadband afterglow observations provide constraints on the explosion energetics, geometry, and immediate environs of the progenitor star. The afterglow has a predictable temporal and spectral evolution that depends on the kinetic energy and geometry of the shock, the density structure of the circumburst environment, and shock microphysical parameters which depend on the physics of particle acceleration and the circumburst magnetic field. To the degree that we can predict differences in the explosion and circumburst media between GRB progenitors at high and low redshifts, we can search for these different signatures in their afterglows. This has been the motivation for previous multi-wavelength modeling of the highest-z afterglows (Frail et al. 2006; Gou et al. 2007).

In order to investigate the nature of the GRB 090423 explosion, we combine our radio measurements with published X-ray and NIR observations, and apply a model of the blast wave evolution to fit the afterglow data (§3). We compare the explosion energetics, circumburst density, and other derived characteristics to a sample of well-studied events, and discuss prospects for using afterglow measurements to investigate the nature of high-z massive star progenitors.

2. Observations

2.1. Radio observations

We began observing a field centered at the NIR afterglow of GRB 090423 with the VLA about one day after the burst (Chandra et al. 2009). Our first detection of the GRB afterglow was not until about one week later at a flux density of 73.8 ± 21.7 μJy. We continued to monitor the GRB with the VLA until it faded below detection on day 64. The flux density scale was tied to 3C 286 and the phase was measured by switching with a 6.5 minute cycle time between the GRB field and the point source calibrator J0954+177. To maximize sensitivity, the full VLA continuum bandwidth (100 MHz) was recorded in two 50 MHz bands. Data reduction was carried out following standard practice in the *AIPS* software package.

In Table 1 we list the *individual* VLA measurements. In order to improve our detection sensitivity, we averaged several adjacent observations. Datasets were combined in the *UV*-plane prior to imaging. By averaging three adjacent epochs (2009 May 1–May 3) when

[1]The Very Large Array is operated by the National Radio Astronomy Observatory, a facility of the National Science Foundation operated under cooperative agreement by Associated Universities, Inc.

the afterglow was brightest, we estimate the best GRB position by fitting a 2-D Gaussian, which is; RA, Dec (J2000): $09^h55^m(33.279\pm0.005)^s$, $18^d08'(57.935\pm0.067)''$. This position is consistent with an earlier, less accurate WFCAM-UKIRT position from Tanvir et al. (2009b).

Table 2 gives the flux densities at the averaged epochs. For all epochs the flux density was measured at the position given above. We plot these data in Fig. 1. There is a broad plateau of about 45 μJy from 12 to 38 days, followed by a decline around day 55. The initial detections on days 8–10 could have contribution from a short-lived reverse shock (§3).

We also observed GRB 090423 with the Combined Array for Research in Millimeter-wave Astronomy (CARMA) at 95 GHz band on 2009 Apr 25.19 UT. The observation was 8 hours in length. Data was obtained under non-ideal weather conditions. The peak flux at the VLA afterglow position is 450± 180 μJy. Castro-Tirado et al. (2009) reported a secure millimeter band detection (λ = 3 mm) at a flux density of 200 μJy with the Plateau de Bure Interferometer (PdBI) observed on 2009 Apr 23 & 24. Riechers et al. (2009) placed flux upper limit of 0.96 mJy in 250 MHz band observed with the Max-Planck-Millimeter Bolometer (MAMBO-2) array at the IRAM 30-m telescope. The Westerbork Synthesis Radio Telescope (WSRT) also observed the GRB between 2009 May 22.48 UT to 23.46 UT at 4.9 GHz and did not detect the afterglow (van der Horst 2009).

2.2. X-ray observations

Swift-XRT (Burrows et al. 2005) observed the field of GRB 090423 for one week in Photon Counting (PC) mode. The XRT light curve is obtained from the on-line repository[2] (Evans et al. 2007). The X-ray spectrum is well-fit by a power-law model with a photon index $\Gamma = 2.05^{+0.14}_{-0.09}$ and a total column density of $N_H = (8.7\pm2.5)\times10^{20}$ cm^{-2} (Tanvir et al. 2009a; Krimm et al. 2009). We converted the $0.3-10.0$ keV counts to a flux density at $E = 1.5\,\mathrm{keV}$ ($\nu_0 = 3.6\times10^{17}\,\mathrm{Hz}$) using the above value for Γ and an unabsorbed count rate conversion of 1 count $= 4.6\times10^{-11}$ erg/cm^2/s.

2.3. Near Infrared Observations

The NIR afterglow was observed by a variety of facilities worldwide; we have used values from Tanvir et al. (2009a). To convert magnitudes to flux densities, we used zero-point measurements from Fukugita et al. (1995). We have incorporated the Galactic extinction

[2]http://www.Swift.ac.uk/xrt_curves

($E(B-V) = 0.029$; Dickey & Lockman 1990) into these results.

3. Results and Afterglow Modelling

Here we combine our radio data with the existing X-ray and NIR data and model the afterglow evolution, interpreting it in terms of the relativistic blast wave model (Meszaros 2006). In this model the afterglow physics is governed by the isotropic kinetic energy of the blast wave shock $E_{K,\rm iso}$, the jet opening angle θ_j, the density of the circumburst medium n, and the microscopic parameters such as electron energy index p, and the fraction of the shock energy density in relativistic electrons ϵ_e and magnetic fields ϵ_B. The afterglow modeling software (Yost et al. 2003) assumes a standard synchrotron forward shock formulation. In the X-ray band, we exclude the data before ~ 3900 s, since it contains a flare which is more likely due to the GRB itself than the afterglow.

It is well known (Sari et al. 1998, 1999; Chevalier & Li 1999) that the afterglow framework allows the above blast wave parameters to be constrained using multi-wavelength light curves. First, we note the constancy of the peak flux density ($F_{\nu,\rm max}$) between the NIR and the radio bands in Fig. 1. If we interpret this as the passage of the synchrotron peak frequency ν_m through each band, this immediately rules out the wind model ($F_{\nu,\rm max} \propto t^{-1/2}$) and favors a constant-density ambient medium ($F_{\nu,\rm max} \propto t^0$). Another related constraint which comes from the Fig. 1 is the time of the peak in the NIR versus the radio bands. We note that in the NIR band, the light curve peaks at ~ 0.08 d. Thus if there was an early jet break the model predicts that the synchrotron peak frequency ν_m would evolve from NIR to radio band around day 10 ($\nu_m \propto t^{-2}$), however, for the isotropic model ν_m should pass through the 8.5 GHz band around ~ 50 days ($\nu_m \propto t^{-3/2}$). Since radio light curve indeed peaks at about 50 d, this confirms that the jet break has not occurred at least until the afterglow peaked in radio band.

Second, the declining part of the IR light curve is well fit by a power law with a decay index $\alpha = -1.10 \pm 0.27$. Whereas the overall X-ray light curve after 3900s is well fit with a power law index of $\alpha = -1.35 \pm 0.15$. For the isotropic, constant density model we expect the flux at a given frequency $\nu_{\rm obs}$ to decline as $t^{3(1-p)/4}$ for $\nu_m < \nu_{\rm obs} < \nu_c$ and $t^{(2-3p)/4}$ for $\nu_m < \nu_c < \nu_{\rm obs}$, where ν_c is the synchrotron cooling frequency (Sari et al. 1998). These relations give consistent values of p for the NIR ($p = 2.46 \pm 0.36$) and X-ray ($p = 2.46 \pm 0.20$).

Finally, having obtained an estimation for p and determining the fact the X-ray frequency has evolved past the cooling frequency $\nu_{\rm X-ray} > \nu_c$, we can put a constraint on the total energy carried by the fireball electrons ($\epsilon_e E$) just from a single X-ray flux measure-

ment. Using Eq. 4 of Freedman & Waxman (2001) and X-ray flux on day 1, we obtain the fireball electron energy per unit solid angle in an opening angle $1/\Gamma$ on $t = 1$ d to be $\epsilon_e E/4\pi = 7.4 \times 10^{51}$ ergs. If we assume $\epsilon_e = 1/3$ (Freedman & Waxman 2001), then the total fireball energy per unit solid angle in this opening will be $E/4\pi = 2.5 \times 10^{52}$ ergs.

We summarize our robust inferences based on this preliminary analysis: (a) the data favors an isotropic explosion in a constant density medium; (b) the cooling frequency lies between the IR and X-ray bands; (c) the afterglow kinetic energy is large. From Tanvir et al. (2009a) we also know that the extinction due to a putative host galaxy is negligible ($A_V < 0.08$).

We now move on to more detailed modeling (Yost et al. 2003) guided broadly by these preliminary results. We fit a constant density model for parameters: $E_{K,\rm iso}$, θ_j, n, p, ϵ_e and ϵ_B. All parameters were allowed to vary freely except that we fixed $p = 2.46$ to lie in a narrow range (± 0.20). The best fit parameters are tabulated in Table 3. Our best fit model is plotted in Fig. 1.

This simple model provides a reasonable fit to the data. The model implies GRB kinetic energy to be $E_K = 3.8 \times 10^{53}$ erg. However, the last measured data point is around day 65 (radio band) and the last detections in the radio and NIR bands are at about day 40 and day 46, respectively. Therefore a late jet break cannot be ruled out by these data. To illustrate this more concretely we overlay our best-fit model in Fig. 1 with a late jet break $t_j \sim 45$ d. The implied jet opening angle $\theta_j > 0.21$ rad reduces both the radiated and the kinetic energies of this event by a factor of ~ 45. In this case the isotropic equivalent gamma-ray energy $\rm E_\gamma = 1 \times 10^{53}$ erg (von Kienlin 2009) and the blastwave kinetic energy $E_K = 3.8^{+9.8}_{-1.7} \times 10^{53}$ erg give *lower limits* to the beaming-corrected values of $E_\gamma > 2.2 \times 10^{51}$ erg and $E_K > 8.4^{+21.6}_{-3.7} \times 10^{51}$ erg, respectively.

The radio data point on day 9.34 ($t \sim 1$ d in the rest frame) has high flux and does not go through the best fit forward shock model. Such early, short-lived radio emission is fairly common in GRBs at lower redshifts and is thought to be due to a contribution from afterglow reverse shock (RS) (Kulkarni et al. 1999; Soderberg & Ramirez-Ruiz 2003; Nakar & Piran 2004). We can make a rough estimate of the peak RS contribution for GRB 090423 using the formulation of Nakar & Piran (2004) and the best fit parameters. The order of magnitude calculation shows that the RS contribution is expected to be ~ 20 μJy. Even though this estimate may have large uncertainties, this does support our speculation that the RS is likely contributed some of the radio emission seen on $t = 9.34$ d. If we assume that the data on day 9.34 represents the peak of the reverse shock then this corresponds to a synchrotron self absorption frequency of $\nu_a^r \sim 3.4 \times 10^{14}$ Hz. Using the scaling law for RS emission, $t_{\rm radio} = \nu_a^r t_o / \nu_{\rm radio}$, the time for RS peak in 90 GHz is $t \sim 0.87$ d. This implies that PdBI

data flux reported by Castro-Tirado et al. (2009) may also have contribution from the RS.

4. Discussion and Conclusions

GRB 090423 is the highest-redshift object for which we have multi-wavelength observations, including good quality radio measurements. Below we address the following questions: based on its afterglow properties what can we learn about properties of the explosion and environs for this highest-redshift GRB? And, can we identify any differences between high and low redshift GRBs which indicate that they might arise from different progenitors? In particular, the initial generations of stars in the early universe are thought to be brighter, hotter and more massive ($> 100\,M_{\odot}$) than stars today (Haiman 2008; Bromm et al. 2009). Detecting these so-called Population III (Pop III) stars is one of the central observational challenges in modern cosmology, and the best prospect appears to be through observing their stellar death (Heger et al. 2003) via a supernovae (SNe) or gamma-ray burst explosion. It is worth asking what observational signatures could signal a Pop III GRB.

Other than GRB 090423, only one other $z > 6$ event, GRB 050904 ($z = 6.26$), has high quality broadband afterglow measurements. In Fig. 2 we plot the best-fit parameters of these two GRBs along with a sample of well-studied lower redshift events from Panaitescu & Kumar (2001). Both high redshift bursts stand out in terms of their large blast wave energy ($> 10^{52}$ erg). We know from samples of well-studied afterglows (Frail et al. 2001; Panaitescu & Kumar 2001; Yost et al. 2003), that most have radiative and kinetic energies of order $\sim 10^{51}$ erg. In the collapsar model the jet kinetic energy from a Pop III GRB could be 10–100 times larger than a Population II (Pop II) event (Fryer et al. 2001; Heger et al. 2003). However, an energetic explosion does not appear to be an exclusive property of high-z GRBs. There is a small but growing population of bursts with energy $> 10^{52}$ erg, termed 'hyper-energetic GRBs' (Cenko et al. 2009), which includes moderate-z events like GRB 070125 (Chandra et al. 2008) and GRB 050820A (Cenko et al. 2006).

Another potentially useful diagnostic is the density structure in the immediate environs of the progenitor star. The radio data is a sensitive *in situ* probe of the density because its emission samples the optically thick part of the synchrotron spectrum. The afterglows of GRB 090423 and GRB 050904 are best fit by a constant density medium and not one that is shaped by stellar mass loss (Chevalier & Li 1999). However, many afterglows at all redshifts are best fit by a constant density medium (e.g. Yost et al. 2003). The density obtained for GRB 050904 was the highest seen ($n \approx 84 - 680$ cm^{-3}) for any GRB to date, while GRB 090423 with $n = 0.9$ cm^{-3} does not stand out (Fig. 2), indicating these two high redshift bursts exploded in very different environments. A circumburst density of order

unity is predicted for Pop III stars, since this density is limited by strong radiation pressure in the mini halo from which the star was formed (Bromm et al. 2003). This is not an unique property, since many local SNe explode in tenuous media, and so density constraints are not useful to signal Pop III explosions.

For the other afterglow parameters (p, ϵ_e, ϵ_B and θ_j) there are no published predictions for how they may differ between different progenitor models. Thus we turn to considering the prompt high-energy emission of GRB 090423.

Salvaterra et al. (2009) and Tanvir et al. (2009a) both noted that the high-energy properties of GRB 090423 (fluence, luminosity, duration, radiative energy) are not substantially different from those moderate-z GRBs. We are not aware of any quantitative predictions based on these observed properties that would discriminate between Pop II and Pop III progenitors. For example, apart from the effect of $(1 + z)$ time dilation, there is no reason to expect high-z GRBs to have significantly longer intrinsic durations. Collapsar models which form black holes promptly through accretion onto the proto-neutron star (Type I) or via direct massive (> 260 $M_\odot$) black hole formation (Type III) have durations set by jet propagation and disk viscosity timescales, respectively (MacFadyen et al. 2001; Fryer et al. 2001), which are ~ 10 s in the rest frame (with large uncertainties; Fryer et al. 2001).

Metallicity can also be an important discriminant. There is a critical metallicity ($Z > 10^{-3.5}\,Z_\odot$) below which high-mass Pop III stars dominate (Bromm et al. 2009; Bromm & Loeb 2006). The contribution of Pop III stars to the co-moving star formation rate is expected to peak around $z = 15$ but their redshift distribution exhibits a considerable spread to $z \sim$7. Thus we might find high-redshift GRBs with Pop III progenitors in "pockets" of low metallicity. Salvaterra et al. (2009) argue for a lower bound of $Z > 0.04\,Z_\odot$ based on their detection of excess soft X-ray absorption by metals along the line of sight, in comparison to the Milky Way column density predicted from H I (21 cm) measurements. We do not consider this a robust measurement as it is sensitive to a range of unaccounted-for systematic effects, including: spectral variability; spectral curvature; low-amplitude X-ray flares; and the presence of intervening (cosmological) absorption systems along the line of sight.

Summarizing the above discussion, we do not find that the individual properties of GRB 090423 are sufficiently dissimilar to other GRBs to warrant identifying it as anything other than a normal GRB. We lack robust predictions of well-defined afterglow signatures that could allow us to unambiguously identify a Pop III progenitor star from its afterglow properties alone. Significantly larger numbers of GRBs at high redshift with well-sampled afterglow light curves, high-resolution spectra, and host galaxy detections are needed to determine if high redshift GRB progenitors differ in a statistical sense from those at low redshift.

We note that, like GRB 050904, the GRB 090423 afterglow indicates the signature of reverse shock (RS) emission in the radio, as seen in the VLA and PdBI data. (Inoue et al. 2007) have studied the expected RS emission at high redshift, and they find that the effects of time dilation almost compensate for frequency redshift , resulting in a near-constant observed peak frequency in the mm band ($\nu \sim 200$ GHz) at a few hours post-event, and a flux at this frequency that is almost independent of redshift. Further, the mm band does not suffer significantly either from extinction (in contrast to the optical) or scintillation (in contrast to the radio). Therefore, detection of mm flux at a few hours post event should be a good method of indicating a high redshift explosion. ALMA, with its high sensitivity ($\sim$75 μJy in 4 min), will be a potential tool for selecting potential high-z bursts that would be high priority for intense followup across the spectrum. This will hopefully greatly increase the rate at which high-z events are identified.

Finally, our data does not rule out a late jet break at $t_j > 45$ d, which, as discussed above, makes the total explosion energy uncertain. Extremely sensitive VLA observations would be required to distinguish between the isotropic versus jet model. However, in 2010 with an order of magnitude enhanced sensitivity the EVLA will be the perfect instrument for such studies. For a 2 hr integration in 8 GHz band, the EVLA can reach sensitivity up to 2.3 μJy which will be able to detect the GRB 090423 for 2 years or 6 months if the burst is isotropic or jet-like, respectively. EVLA will thus be able detect fainter events and follow events like GRB 050904 and GRB 090423 for a longer duration, therefore obtaining better density measurements, better estimates of outflow geometry and the total kinetic energy.

We thank Bob Dickman for his generous allocation of VLA time and Joan Wrobel and Mark Claussen for the timely scheduling of the observations. This work made use of data supplied by the UK Swift Science Data Centre at the University of Leicester.

REFERENCES

Bromm, V. & Loeb, A. 2006, ApJ, 642, 382

Bromm, V., Yoshida, N., & Hernquist, L. 2003, ApJ, 596, L135

Bromm, V., Yoshida, N., Hernquist, L., & McKee, C. F. 2009, Nature, 459, 49

Burrows, D. N., Hill, J. E., Nousek, J. A., et al. 2005, Space Science Reviews, 120, 165

Castro-Tirado, A. J., Bremer, M., Winters, J.-M., et al. 2009, GCN Circ., 9273, 1

Cenko, S. B., Frail, D. A., Harrison, F. A., et al. 2009, ApJ, submitted (astro-ph/0905.0690)

Cenko, S. B., Kasliwal, M., Harrison, F. A., et al. 2006, ApJ, 652, 490

Chandra, P., Cenko, S. B., Frail, D. A., et al. 2008, ApJ, 683, 924

Chandra, P., Frail, D. A., & Kulkarni, S. R. 2009, GCN Circ., 9249, 1

Chevalier, R. A. & Li, Z.-Y. 1999, ApJ, 520, L29

Ciardi, B. & Loeb, A. 2000, ApJ, 540, 687

Dickey, J. M. & Lockman, F. J. 1990, ARA&A, 28, 215

Evans, P. A., Beardmore, A. P., Page, K. L., et al. 2007, A&A, 469, 379

Frail, D. A., Cameron, P. B., Kasliwal, M., et al. 2006, ApJ, 646, L99

Frail, D. A., Kulkarni, S. R., Sari, R., et al. 2001, ApJ, 562, L55

Freedman, D. L. & Waxman, E. 2001, ApJ, 547, 922

Fryer, C. L., Woosley, S. E., & Heger, A. 2001, ApJ, 550, 372

Fukugita, M., Shimasaku, K., & Ichikawa, T. 1995, PASP, 107, 945

Gou, L.-J., Fox, D. B., & Mészáros, P. 2007, ApJ, 668, 1083

Gou, L. J., Mészáros, P., Abel, T., & Zhang, B. 2004, ApJ, 604, 508

Greiner, J., Krühler, T., Fynbo, J. P. U., et al. 2009, ApJ, 693, 1610

Haiman, Z. 2008, Astrophysics & Space Science Library, Eds. H. Thronson, A. Tielens, M. Stiavelli, Springer (astro-ph/0809.3926)

Heger, A., Fryer, C. L., Woosley, S. E., et al. 2003, ApJ, 591, 288

Inoue, S., Omukai, K., & Ciardi, B. 2007, MNRAS, 380, 1715

Kawai, N., Kosugi, G., Aoki, K., et al. 2006, Nature, 440, 184

Krimm, H. A., Pasquale, M. D., Perri, M., et al. 2009, GCN Rep., 211

Kulkarni, S. R., Frail, D. A., Sari, R., et al. 1999, ApJ, 522, L97

Lamb, D. Q. & Reichart, D. E. 2000, ApJ, 536, 1

MacFadyen, A. I., Woosley, S. E., & Heger, A. 2001, ApJ, 550, 410

Meszaros, P. 2006, Reports of Progress in Physics, 69, 2259

Nakar, E. & Piran, T. 2004, MNRAS, 353, 647

Panaitescu, A. & Kumar, P. 2001, ApJ, 554, 667

Perley, D. A., Cenko, S. B., Bloom, J. S., et al. 2009, AJ, submited (astro-ph/0905.0001)

Riechers, D. A., Walter, F., Bertoldi, F., et al. 2009, GCN Circ., 9322, 1

Salvaterra, R., Della Valle, M., Campana, S., et al. 2009, Nature, accepted (astro-ph/0906.1578)

Sari, R., Piran, T., & Halpern, J. P. 1999, ApJ, 519, L17

Sari, R., Piran, T., & Narayan, R. 1998, ApJ, 497, L17+

Soderberg, A. M. & Ramirez-Ruiz, E. 2003, MNRAS, 345, 854

Tanvir, N. R., Fox, D. B., Levan, A. J., et al. 2009a, Nature, accepted (astro-ph/0906.1577)

Tanvir, N., Levan, A., Kerr, T., & Wold, T. 2009b, GCN Circ., 9202, 1

Totani, T., Kawai, N., Kosugi, G., et al. 2006, PASJ, 58, 485

van der Horst, A. J. 2009, GCN Circ., 9503, 1

von Kienlin, A. 2009, GCN Circ., 9251, 1

Woosley, S. E. & Bloom, J. S. 2006, ARA&A, 44, 507

Yost, S. A., Harrison, F. A., Sari, R., & Frail, D. A. 2003, ApJ, 597, 459

Table 1. Radio observations of GRB 090423

Date UT	Δt days	Tel.	Freq. GHz	F_ν[a] μJy	Int. time[b]	Array Conf.
Apr 25.01	1.68	VLA	8.46	51 ± 45	13	B
Apr 26.08	2.75	VLA	8.46	-17 ± 37	16	B
May 01.05	7.72	VLA	8.46	74 ± 22	50	B
May 03.08	9.75	VLA	8.46	77 ± 18	75	B
May 03.98	10.65	VLA	8.46	57 ± 19	75	B
May 05.05	11.72	VLA	8.46	38 ± 19	71	B
May 05.99	12.66	VLA	8.46	87 ± 23	56	B
May 08.09	14.76	VLA	8.46	-4 ± 19	67	B
May 09.05	15.72	VLA	8.46	5 ± 18	71	B
May 10.08	16.75	VLA	8.46	73 ± 18	71	B
May 12.99	19.66	VLA	8.46	29 ± 18	70	B
May 14.10	20.77	VLA	8.46	88 ± 21	45	B
May 15.05	21.72	VLA	8.46	7 ± 15	110	B
May 20.13	26.80	VLA	8.46	42 ± 18	78	B
May 27.12	33.79	VLA	8.46	78 ± 19	77	BnC
Jun 01.11	38.78	VLA	8.46	44 ± 18	77	BnC
Jun 20.00	57.67	VLA	8.46	19 ± 21	78	C
Jun 26.08	63.75	VLA	8.46	49 ± 19	78	C
Jun 26.91	64.58	VLA	8.46	-4 ± 20	75	C
Apr 25.20	1.87	CARMA	92.5	450 ± 180	...	...

[a]Peak flux density at GRB 090423 position.

[b]Integration time on GRB 090423 in minutes.

Table 2. VLA 8.5 GHz flux densities of GRB 090423 at combined epochs

Epochs Combined	Days since explosion	Flux density μJy
Apr 25.01–Apr 26.08	2.21 ± 0.54	50.9 ± 30.9
May 01.05–May 03.98	9.34 ± 1.64	66.4 ± 11.4
May 05.05–May 10.08	14.32 ± 2.60	43.7 ± 8.9
May 12.99–May 15.05	20.71 ± 1.06	42.2 ± 10.6
May 20.13–Jun 01.11	33.12 ± 6.32	49.6 ± 11.0
Jun 20.00–Jun 26.91	62.00 ± 4.33	7.8 ± 11.6

Table 3. Best fit parameters for multiwaveband modeling of GRB 090423 for $p = 2.46 \pm 0.2$

Parameters	Isotropic	Jet ($t_j > 45$ d)
E_γ (ergs)	1.0×10^{53}	$> 2.2 \times 10^{51}$
E_K (ergs)	$3.8^{+9.8}_{-1.7} \times 10^{53}$	$> 8.4^{+21.6}_{-3.7} \times 10^{51}$
n (cm^{-3})	$0.90^{+0.11}_{-0.06}$	...
$\epsilon_B(\%)$	$0.016^{+0.024}_{-0.015}$	...
ϵ_e	$0.28^{+0.10}_{-0.01}$	...

Note. — For jet model ($t_j > 45$ d), the n, ϵ_B and ϵ_e were fixed to the best fit isotropic model values.

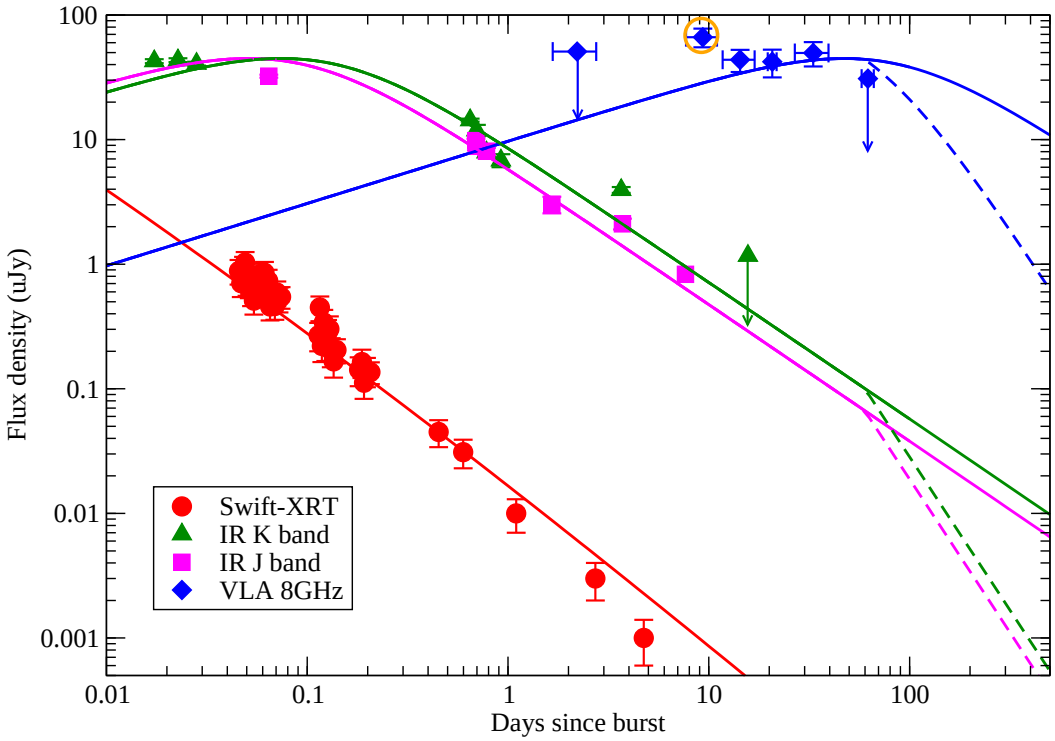

Fig. 1.— Multiwaveband observations for GRB 090423. The solid lines are best fit light curves for constant density isotropic model. The orange circled radio data likely has a contribution from RS (§3). Dashed lines show model with a possible jet break around $t_j = 45$ d.

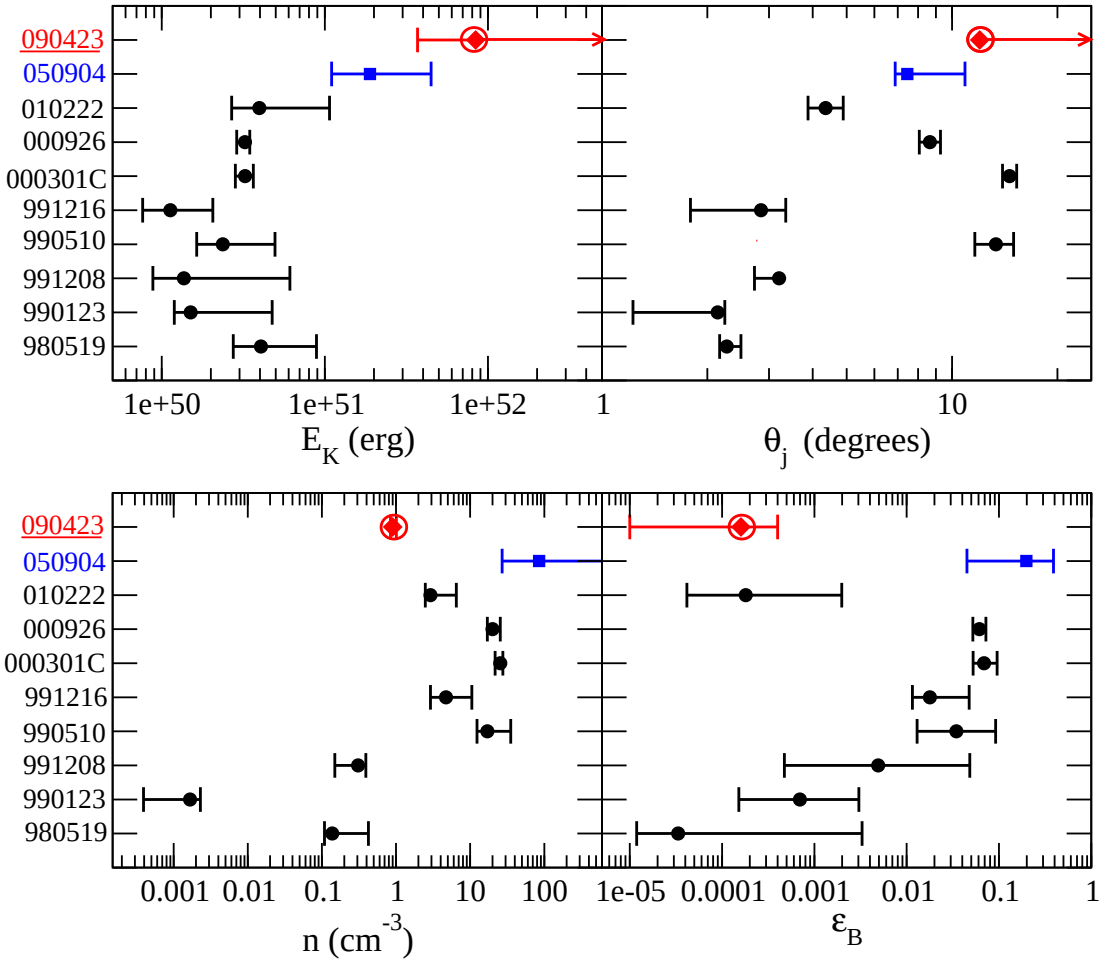

Fig. 2.— Comparison of GRB 090423 best fit parameters with few moderate-z GRBs ($z \sim 1-3$) from Panaitescu & Kumar (2001) and with the high-z GRB 050904 ($z = 6.295$, Gou et al. 2007; Frail et al. 2006). Here the upper limit on GRB 090423 E_K is $(3.8 + 9.8) \times 10^{51}$ erg.